



University of  
Massachusetts  
Amherst

## 4 Co Outflows And Dense Gas In The Dark Cloud Complex Near Ic5146

Item Type	Article
Authors	Dobashi, Kazuhito;Onishi, Toshikazu;Iwata, Takahiro;Nagahama, Tomoo;Patel, Nimesh;Snell, Ronald L.;Fukui, Yasuo
DOI	<a href="https://doi.org/10.1086/116527">10.1086/116527</a>
Download date	2026-03-05 11:34:14
Link to Item	<a href="https://hdl.handle.net/20.500.14394/3326">https://hdl.handle.net/20.500.14394/3326</a>

FOUR CO OUTFLOWS AND DENSE GAS IN THE DARK CLOUD COMPLEX  
NEAR IC5146

KAZUHITO DOBASHI

Materials Science, University of Osaka Prefecture, Sakai 593, Osaka, Japan

TOSHIKAZU ONISHI

Department of Astrophysics, Nagoya University, Nagoya 464-01, Japan

TAKAHIRO IWATA

Kashima Space Research Center, Communications Research Laboratory, Kashima, Japan

TOMOO NAGAHAMA

Department of Astrophysics, Nagoya University, Nagoya 464-01, Japan

NIMESH PATEL AND RONALD L. SNELL

Five College Radio Astronomy Observatory, and Department of Physics and Astronomy, University of Massachusetts, Amherst, Massachusetts 01003

YASUO FUKUI

Department of Astrophysics, Nagoya University, Nagoya 464-01, Japan

Received 1992 August 4; revised 1992 November 16

ABSTRACT

We report an outflow survey carried out in the dark cloud complex near IC5146 open cluster using the  $^{12}\text{CO}(J=1-0)$  emission line. The observations were carried out with a 15 element imaging array at the FCRAO (QUARRY). An area of about 130 square arcmin was searched for outflows, corresponding to 17% of the extent of the  $^{13}\text{CO}$  cloud and 40% of that of the  $\text{C}^{18}\text{O}$  cloud. Four regions exhibiting high velocity CO wings were newly found, and each of them is associated with *IRAS* point sources.  $\text{C}^{18}\text{O}(J=1-0)$  observations were also made with the Nagoya 4 m radio telescope toward the most massive member of the molecular cloud complex, in which the four outflows are located. The outflow sources are found to be surrounded by the dense gas which mean molecular number density is  $\sim 1 \times 10^3 \text{ cm}^{-3}$ , although they tend to be located in the less dense parts of the  $\text{C}^{18}\text{O}$  cloud, not toward the  $\text{C}^{18}\text{O}$  peaks. The  $\text{C}^{18}\text{O}$  cloud has a molecular mass of  $\sim 1600 M_{\odot}$ , similar to that of the Taurus cloud complex,  $\sim 1200 M_{\odot}$ , and the typical  $\text{C}^{18}\text{O}$  linewidth,  $1.5 \text{ km s}^{-1}$ , is significantly larger than that in the Taurus cloud,  $1.0 \text{ km s}^{-1}$ , convolved to the same spatial resolution,  $\sim 0.8 \text{ pc}$ . The FIR luminosities of the protostar candidates in the IC5146 region,  $\sim 4 L_{\odot}$  up to  $160 L_{\odot}$ , are considerably greater than those in Taurus,  $\sim 10 L_{\odot}$ . These comparisons indicate that the IC5146 region is characterized by a higher mass star formation and larger velocity dispersion than the Taurus cloud complex.

1. INTRODUCTION

A young open cluster, IC5146, with a small H II region (S125) is located in Cygnus. IC5146 is accompanied by several Lynds clouds (Lynds 1962) within  $\sim 2^{\circ}$  west. Various observations of the open cluster itself and its surrounding gas have been made in 21 cm (H I measurement carried out by Riegel 1967; Israel 1977; Roger & Irwin 1982) and in  $^{12}\text{CO}(J=1-0)$  and  $^{13}\text{CO}(J=1-0)$  (Millman *et al.* 1975; Lada & Elmegreen 1979; McCutcheon *et al.* 1982).

Infrared observations to search for young stellar objects were carried out by Elias (1978) and Wilking *et al.* (1984). Elias found two protostar candidates. One is BD +46°3471 found  $\sim 10'$  west of the open cluster, and the other is Elias 1-12, both of which are known to be CO outflow sources (Levreault 1983, 1988). The cloud associ-

ated with Elias 1-12 is located further west from IC5146 by  $\sim 1^{\circ}$ . The *IRAS* survey revealed that at least six protostar candidates, including Elias 1-12, are embedded in this cloud, suggesting that star formation is going on inside of it. Recent CO and  $^{13}\text{CO}$  observations have shown that this cloud is the most massive member in the dark cloud complex, mainly consisting of two  $^{13}\text{CO}$  clumps with a total mass of  $\sim 2 \times 10^3 M_{\odot}$  (Dobashi *et al.* 1992, hereafter referred to as Paper I). A virial analysis of these clumps indicates that they are gravitationally stable, suggesting the existence of internal supporting force against gravity.

Molecular outflows are important signature of recent star formation (e.g., Lada 1985; Snell 1987; Fukui 1989; Fukui *et al.* 1992). It is interesting to see if the protostar candidates located in this cloud show outflows. No observations to search for the outflows in this region have been done, except for the two objects (BD+46°3471 and Elias

TABLE 1. Observed *IRAS* sources.

Object <sup>a</sup>	<i>IRAS</i> No.	Position		Flux Density				C.C.	L <sup>b</sup> (L <sub>⊙</sub> )	Optical <sup>c</sup> counterpart	Comments
		α(1950) (h m s)	δ(1950) (° ' ")	F12 (Jy)	F25 (Jy)	F60 (Jy)	F100 (Jy)				
7	21428+4732	21 42 51.2	47 32 55	<1.12	0.31	1.60	<18.50	NFBA	<4	C	
8	21429+4726	21 42 59.2	47 26 40	<0.25	1.73	10.95	18.50	LAAA	35	F	
9	21432+4719	21 43 17.3	47 19 30	<0.25	1.42	12.19	23.45	AAA	40	F	
10	21441+4722	21 44 06.2	47 22 11	<0.31	0.57	1.48	<11.78	JBAD	<5	F	
11	21454+4718	21 45 28.0	47 18 13	2.40	8.04	40.0	83.53	AAAA	157	V	Elias1-12 <sup>d</sup>
12	21461+4722	21 46 06.6	47 22 40	<0.25	0.42	2.43	7.44	CAB	11	...	
16	21445+4704	21 44 35.6	47 04 21	<0.25	<0.34	0.86	13.43	EDBD	12	F	L1031C <sup>e</sup>

note :

a Numbers in this column are quoted from Dobashi et al.(1992), and the sources are identified by these numbers in Fig.7.

b The values in this column are the upper limits of the luminosities (based on Myers et al. 1987).

c Optical counterparts on Palomar Sky Survey print (red); V: visible star, F: faint, C: contaminated.

d Elias1-12 is already known to be an outflow source (Levreault 1983), and is not observed in the present outflow survey.

e Beichman et al. (1986).

1–12). In this paper, we report the results of a search for CO outflows, and the discovery of four outflow sources in this cloud. We also present results of C<sup>18</sup>O(*J*=1–0) observations which were made to obtain better estimates of the mass of the cloud than those derived from our previous <sup>13</sup>CO observations.

## 2. OBSERVATIONS

### 2.1 <sup>12</sup>CO Observations: Outflow Survey

<sup>12</sup>CO(*J* = 1–0) observations were made with the 14 m telescope at FCRAO for five days in 1992 January. The telescope was equipped with a 15 element imaging array consisting of cryogenic Schottky diode mixers (Erickson *et al.* 1992). Each element has a beam size of 0.9' at FWHM. The receivers provided typical system temperature of 600 K for <sup>12</sup>CO(*J* = 1–0) in single side band, including the atmosphere toward the zenith. The spectrometer was a filter bank giving a velocity resolution and a velocity coverage of 0.65 and 20 km s<sup>–1</sup>, respectively.

<sup>12</sup>CO data were taken by position switching to detect weak emission of molecular outflows. The rms values of the obtained data were ~0.1 K. The six selected *IRAS* point sources listed in Table 1 were mapped with a 50" grid, except Elias 1–12 which was previously observed by Levreault (1983). More than 30 spectra were obtained in an area larger than 200"×250" around each object to search for the associated high velocity lobes.

Objects 8 and 12 in Table 1 were observed to check the receiver stability and to determine the absolute temperature scale, *T<sub>R</sub>*<sup>\*</sup>, by assuming antenna temperatures of 8.0 and 6.0 K, respectively (Paper I).

### 2.2 C<sup>18</sup>O Observations

C<sup>18</sup>O(*J*=1–0) data were obtained with the new 4 m millimeter telescope at Nagoya University for two weeks in 1992 February. The beam size of the telescope at 110 GHz is 2.7'. The system temperature of the 4 K cooled Nb

superconductor insulator superconductor (SIS) mixer receiver was typically around 300 K for C<sup>18</sup>O(*J*=1–0) in single side band toward the zenith. The details of the SIS receiver are described elsewhere (Ogawa *et al.* 1990). The spectrometer was an acousto-optical spectrometer which gives a velocity resolution and a velocity coverage of 0.1 and 100 km s<sup>–1</sup>, respectively.

The C<sup>18</sup>O mapping was made with a 2' grid for an area of ~0.3°×0.6° in the dark cloud complex (as shown in Fig. 7). Frequency switching technique with a frequency interval of 13 MHz was used to obtain the data. S140 was observed every 2 h to check the receiver stability. We also observed the position α(1950)=16<sup>h</sup>23<sup>m</sup>46.0<sup>s</sup>, δ(1950)=–24°25'44" in the ρ-Oph region to determine the absolute temperature scale, *T<sub>R</sub>*<sup>\*</sup>, by assuming an antenna temperature of 6.2 K (Wilking & Lada 1983). The rms noise fluctuations of the obtained spectra are ~0.1 K for 0.1 km s<sup>–1</sup> resolution and ~6 min integration time.

## 3. RESULTS AND DISCUSSION

### 3.1 Four CO Outflows

The outflow survey in the <sup>12</sup>CO(*J* = 1–0) line was made for six protostar candidates in the region within 21<sup>h</sup>42<sup>m</sup> < α(1950) < 21<sup>h</sup>46<sup>m</sup> and 47°00' < δ(1950) < 47°40'. The objects were selected from the *IRAS* point sources catalog (*IRAS Point Source Catalog* 1988) with the following selection criteria: (1) sources detected in at least two bands including 60 μm, (2) sources with higher flux densities in 60 μm band than in 25 μm, and (3) sources having <sup>13</sup>CO(*J* = 1–0) emission greater than 3 K km s<sup>–1</sup> (Paper I). There remain seven *IRAS* point sources under the above criteria as listed in Table 1. Throughout this paper, the selected sources are identified by numbers from 7 to 16 given in the first column of the table, which are quoted from Paper I. Elias 1–12 is included in the table, which is known to be an outflow source (Levreault 1983) and thus was not observed here.

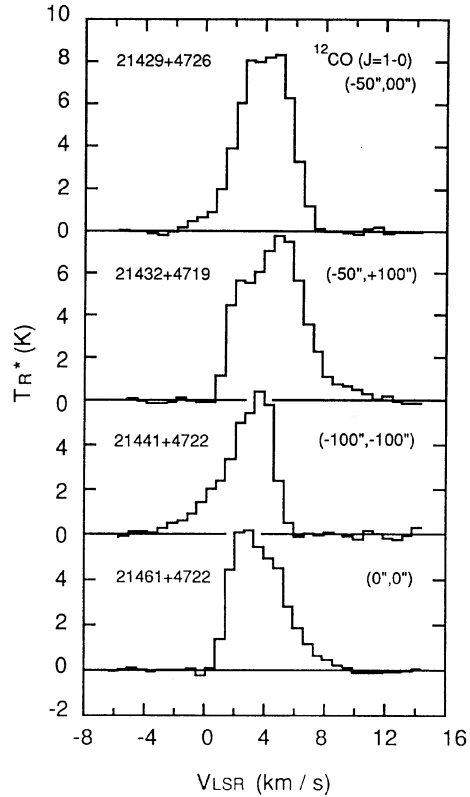


FIG. 1.  $^{12}\text{CO}$  profiles of four discovered molecular outflows. The profiles are taken where the blue or red wing intensities are prominent. Their positions are indicated by the offset ( $\Delta\text{R.A.}$ ,  $\Delta\text{Dec.}$ ) from each associated *IRAS* source.

Out of the six *IRAS* sources, four objects have been newly found to be outflow sources (Obj.8, 9, 10, and 12), and the other two were not confirmed to be outflows because of somewhat curved baselines. Figure 1 shows typi-

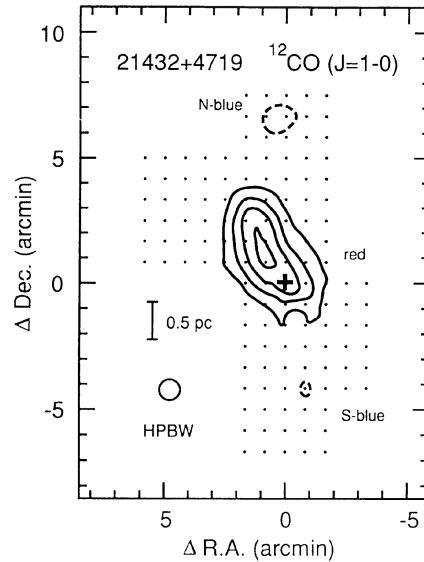


FIG. 2. A contour map of wing components in the direction of 21432+4719. The source has a large red wing (solid lines) and two small blue wings (broken lines). Integration intervals are from  $-3.0$  to  $0.0$   $\text{km s}^{-1}$  and from  $7.0$  to  $11.0$   $\text{km s}^{-1}$  for the blue and red wings, respectively. Contours start from  $1.0$   $\text{K km s}^{-1}$  with increments of  $1.0$   $\text{K km s}^{-1}$ . The source 21432+4719 is denoted by a plus, and dots mark the observed positions.

cal profiles of the outflows. The blue and red wings appear in the range of  $(-3,0)$  and  $(7,11)$   $\text{km s}^{-1}$  in the local standard of rest (LSR) velocity, respectively. Observed properties of the wing emission are summarized in Table 2, and spatial distributions of red and blue lobes of each object are shown in Fig. 2 and Figs. 4 to 6. Parameters of Elias 1–12 are quoted from Levreault (1983) and are also given in the table for comparison. On the basis of the data

TABLE 2. Observed parameters of outflows.

Object <sup>a</sup>	<i>IRAS</i> No.	$T_{\text{R}}^*$ (K)	$V_{\text{LSR}}$ ( $\text{km s}^{-1}$ )	Red				Blue				Comments
				$V_{\text{red}}^b$ ( $\text{km s}^{-1}$ )	$\int T_{\text{R}}^* dv^b$ ( $\text{K km s}^{-1}$ )	Size <sup>c,d</sup> ( $\text{pc} \times \text{pc}$ )	$R^{c,e}$ (pc)	$V_{\text{blue}}^b$ ( $\text{km s}^{-1}$ )	$\int T_{\text{R}}^* dv^b$ ( $\text{K km s}^{-1}$ )	Size <sup>c,d</sup> ( $\text{pc} \times \text{pc}$ )	$R^{c,e}$ (pc)	
8	21429+4726	8.0	3.6	(7.0, 11.0)	2.6	$0.3 \times 0.3$	0.2	(-2.0, 0.5)	1.2	$0.3 \times 0.6$	0.6	
9	21432+4719	7.6	3.6	(7.0, 12.0)	4.5	$1.0 \times 1.7$	1.3	(-3.0, 0.0)	1.3	$0.3 \times 0.3$	2.1	N-blue
								(-3.0, 0.0)	0.9	$0.3 \times 0.3$	1.4	S-blue
10	21441+4722	6.4	3.6	(7.0, 10.0)	0.6	$0.2 \times 0.2$	0.4	(-3.5, 0.0)	2.3	$0.5 \times 0.9$	1.2	
11	21454+4718	...	3.6	(6.8, 17.2)	18.5	$0.5 \times 0.5$	0.3	(-7.5, 0.3)	...	...	...	Elias1-12 <sup>f</sup>
12	21461+4722	6.0	3.6	(6.0, 10.0)	2.9	$0.2 \times 0.3$	0.2	...	...	...	...	

note :

- Numbers in this column are quoted from Table 4 in Dobashi et. al (1992). The *IRAS* sources are identified by these numbers in Fig.7.
- The velocity coverage of the spectrometer may not be wide enough to cover whole the wing components of the outflows. So the velocity intervals and the integrated intensities are lower limits to the actual value.
- The distance is assumed to be 1 kpc (Walker 1959).
- Sizes of the blue and red lobes are defined at FWHM level of the integrated intensity maps of each outflow.
- The radius is defined at the maximum separation between the FWHM contour of the wing emissions and the position of the *IRAS* source.
- The data about Elias1-12 are quoted from Levreault (1983).

TABLE 3. Derived properties of outflows.

Object <sup>a</sup>	IRAS No.	Wing	$N(^{12}\text{CO})$ <sup>b,c</sup> ( $\times 10^{15} \text{ cm}^{-2}$ )	$N(\text{H}_2)$ <sup>b,c</sup> ( $\times 10^{19} \text{ cm}^{-2}$ )	Mass <sup>b</sup> ( $M_{\odot}$ )
8	21429+4726	red	0.9	0.9	0.05
		blue	4	4	0.05
9	21432+4719	red	10	10	2
		N-blue	4	4	0.03
		S-blue	3	3	0.01
10	21441+4722	red	2	2	0.006
		blue	7	7	0.2
d 11	21454+4718	red	...	...	1.2
12	21461+4722	red	9	9	0.05

note :

- a Numbers in this column are quoted from Table 4 in Dobashi et al (1992). The IRAS sources are identified by these numbers in Fig.7.  
 b The velocity coverage of the spectrometer may not be wide enough to cover whole the wing components of the outflows. So the quantities in these columns are lower limits to the actual value.  
 c The optical depth of  $^{12}\text{CO}$  is assumed to be  $\approx 4$  on the average. This value is calculated from the ratio of  $T(^{12}\text{CO})/T(^{13}\text{CO}) \approx 20$  in the red lobe of Elias1-12 (Levreault 1983). The ratio of  $[\text{H}_2]/[^{12}\text{CO}]$  is assumed to be  $1 \times 10^4$ .  
 d Elias1-12 (Levreault 1983).

in Table 2, we derived  $\text{H}_2$  and  $^{12}\text{CO}$  molecular column densities and masses of the outflows. They are listed in Table 3. Other parameters such as mechanical luminosities or dynamical time scales were not estimated because of the limited velocity coverage of the spectrometer, as described in the last paragraph of this section. The column densities

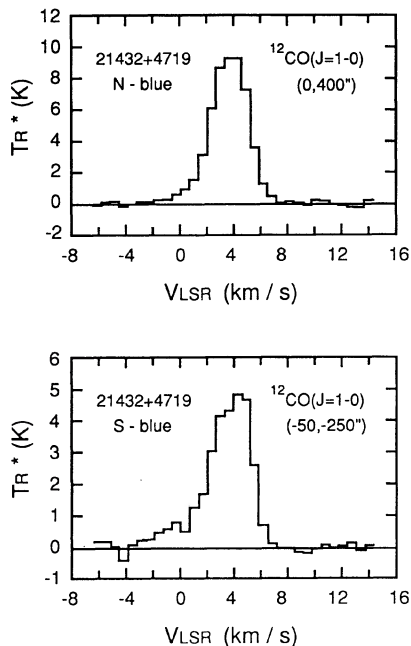


FIG. 3.  $^{12}\text{CO}$  profiles of N-blue and S-blue lobes near 21432+4719. The positions are indicated by the offset ( $\Delta\text{R.A.}$ ,  $\Delta\text{Dec.}$ ) from the associated IRAS source. N-blue lobe is located in the same direction as the giant red lobe from the central IRAS source, indicating that N-blue may originate from another source which is not detected by the IRAS survey (see text).

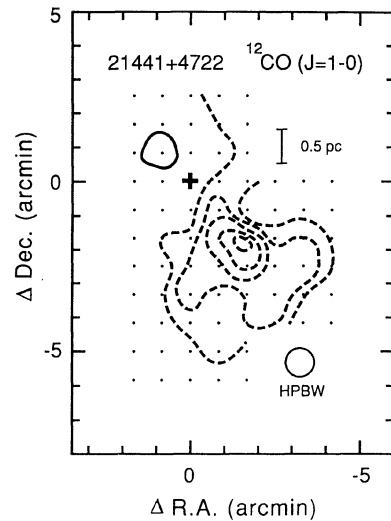


FIG. 4. A contour map of wing components in the direction of 21441+4722. The blue (broken lines) and the red (solid lines) wings are integrated from  $-3.0$  to  $0.0 \text{ km s}^{-1}$  and from  $7.0$  to  $10.0 \text{ km s}^{-1}$ , respectively. Contours start from  $0.4$  with a  $0.4 \text{ K km s}^{-1}$  step. The source 21441+4722 is denoted by a plus, and dots mark the observed positions.

of  $\text{H}_2$  and  $^{12}\text{CO}$  molecules contained in the outflow components were calculated by assuming a mean  $^{12}\text{CO}$  ( $J=1-0$ ) optical depth of 4, as described in detail in the Appendix.

The most impressive outflow among the four is Obj.9, namely IRAS 21432+4719, which is shown in Fig. 2. This object has the most massive and largest red lobe in the observed region with a mass of  $\sim 2 M_{\odot}$  and an extent of  $\sim 1.0 \times 1.7 \text{ pc}^2$ . We found two blue lobes which are significantly smaller than the red lobe. The two blue lobes are located in the opposite sides of the IRAS source. We named them N-blue and S-blue, respectively, according to their positions relative to the IRAS source. Their profiles are shown in Fig. 3. Red and blue lobes are generally symmetric, and it is difficult to explain the existence of the N-blue lobe, as it is on the side of the red lobe. The N-blue lobe may originate from another embedded source which was not found in the IRAS survey which detection limit is about  $10 L_{\odot}$  in the IC5146 region.

For the other three outflows, we show the detailed descriptions below.

**Obj.10 (21441+4722).** Obj.10 is accompanied by a relatively large blue lobe of  $\sim 0.5 \times 0.9 \text{ pc}^2$ , and a small red lobe detected in one beam in the north-east from the IRAS source (Fig. 4). The blue lobe of this object was not covered completely by the present mapping. The total mass of the wing components is estimated to be  $\sim 0.2 M_{\odot}$ .

**Obj.8 (21429+4726).** Both the blue and red lobes were found around this object, whose extents are  $\sim 0.6$  and  $\sim 0.3 \text{ pc}$ , respectively (Fig. 5). The lobes are much smaller than those of Obj.9 in extent and in mass, although the

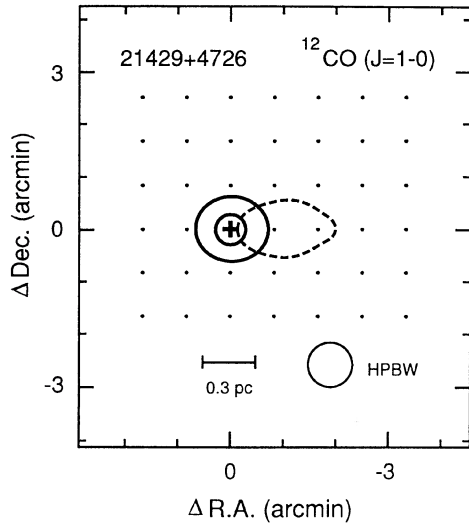


FIG. 5. A contour map of wing components in the direction of 21429+4726. The blue wing (broken lines) and the red wing (solid lines) are integrated from  $-2.0$  to  $0.5 \text{ km s}^{-1}$  and from  $7.0$  to  $11.0 \text{ km s}^{-1}$ , respectively. Contours start from  $0.6 \text{ K km s}^{-1}$  with a  $1.0 \text{ K km s}^{-1}$  step. The source 21429+4726 is denoted by a plus, and dots mark the observed positions.

associated *IRAS* sources are very similar to each other in terms of spectra and flux densities (see Table 1).

**Obj.12 (21461+4722).** The red wing was detected only at the position of the *IRAS* source (Fig. 6). This outflow is not resolved with the present beam size,  $0.9'$  ( $\sim 0.3 \text{ pc}$  at

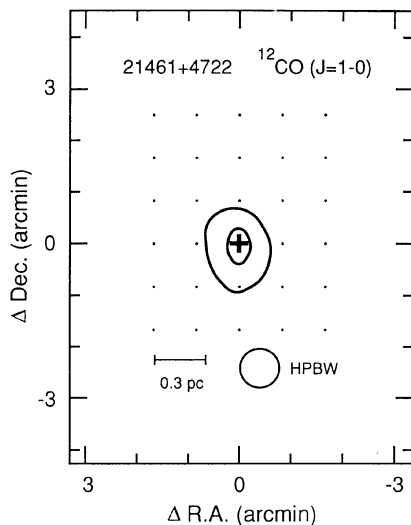


FIG. 6. A contour map of a wing component in the direction of 21461+4722. The source has a compact red wing (solid line) right in the center. The wing is integrated from  $6.0$  to  $10.0 \text{ km s}^{-1}$ . Contours start from  $1.0 \text{ K km s}^{-1}$  with a  $1.0 \text{ K km s}^{-1}$  step. The source 21461+4722 is denoted by a plus, and dots mark the observed positions.

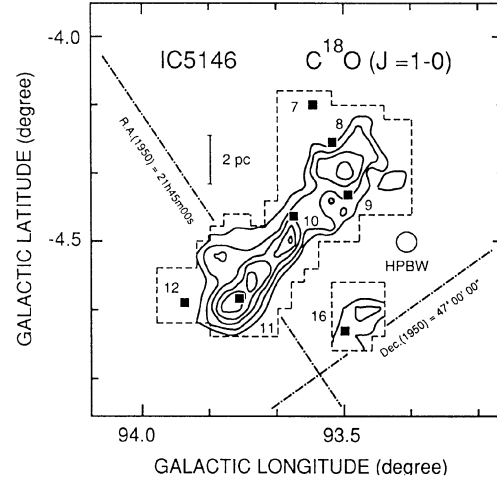


FIG. 7. An integrated intensity map of  $\text{C}^{18}\text{O}(J=1-0)$  shown in galactic coordinates. Contours start from  $0.32 \text{ K km s}^{-1}$  with increments of  $0.16 \text{ K km s}^{-1}$ . The broken line denotes the observed area. Protostar candidates, i.e., selected *IRAS* sources listed in Table 1 are shown by filled squares.

a distance of  $1 \text{ kpc}$ ), and thus, observations with a higher angular resolution will be necessary to investigate its structure.

We note that the velocity coverage of the spectrometer may not be large enough to cover the entire wing emission; e.g., the known outflow source Elias 1–12 has a  $^{12}\text{CO}$  velocity extent of  $\sim 24 \text{ km s}^{-1}$ . So, observed parameters such as the velocity intervals and the integrated intensities of the wing emission may be underestimated, and thus the derived column densities of  $\text{H}_2$  molecules and masses may be lower limits (Tables 2 and 3). Observations with a wider coverage in velocity should be made to better estimate outflow properties.

### 3.2 Distributions of Dense Gas around the Outflows

Our previous  $^{13}\text{CO}$  observations show that the  $^{13}\text{CO}$  peak optical depth is larger than 1 in some parts of the cloud where the five outflows including Elias 1–12 are located. This suggests that the  $^{13}\text{CO}$  line is saturated. In order to better estimate the mass of the cloud, we made observations with the new  $4 \text{ m}$  telescope at Nagoya University in the  $\text{C}^{18}\text{O}(J=1-0)$  emission line which optical depth is much smaller than that of  $^{13}\text{CO}$ . Figure 7 shows the integrated  $\text{C}^{18}\text{O}$  intensity map and the location of the sources listed in Table 1. The figure shows the clumpy structure of the cloud. Most of the sources are located where  $\text{C}^{18}\text{O}$  emission is strong. Although Objs.7 and 12 are not inside  $\text{C}^{18}\text{O}$  contours,  $\text{C}^{18}\text{O}$  temperature of  $\sim 0.2 \text{ K}$  is detected around these objects in one beam of the  $4 \text{ m}$  telescope ( $2.7'$ , i.e.,  $\sim 0.8 \text{ pc}$  at a distance of  $1 \text{ kpc}$ ).

In order to derive physical properties of the cloud, we tentatively identified  $\text{C}^{18}\text{O}$  clumps. The criteria for the identification are the following: (1) the clumps having an integrated intensities more than  $0.6 \text{ K km s}^{-1}$  at their

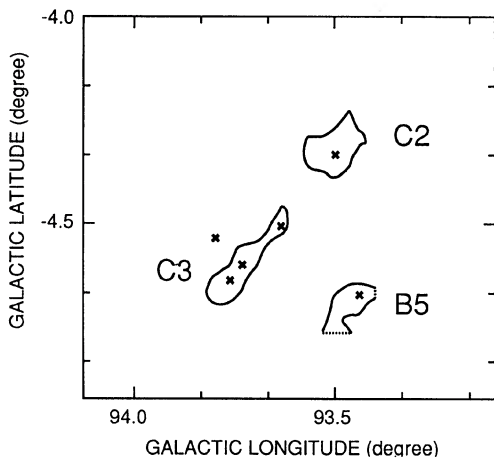


FIG. 8. Location of the three  $C^{18}O$  clumps are shown. Solid lines are FWHM contour levels of the clumps. The names refer to  $^{13}CO$  clumps described in Dobashi *et al.* (1992). The peak positions listed in Table 4 are denoted by the crosses. The clumps have  $C^{18}O$  integrated intensities greater than  $0.5 \text{ K km s}^{-1}$  at the peaks, and are separated from each other at a 50% level of their peaks.

peaks, and (2) the peaks of the clumps are separated from nearby peaks at the contour level of 50% of the peak intensities. As a result, three clumps are identified which are shown in Fig. 8 by their FWHM contour levels. These clumps are located nearly at the same positions as  $^{13}CO$  clumps which were identified by Paper I. So, in this paper, we give the three  $C^{18}O$  clumps names corresponding to  $^{13}CO$  clumps, namely B5, C2, and C3 (see Fig. 8). Observed and derived parameters of the clumps are summarized in Tables 4 and 5, respectively. The  $C^{18}O$  column densities are derived on the assumption that the clumps are in local thermal equilibrium. The calculations were made using

$$N(C^{18}O) = 2.42 \times 10^{14} \frac{\tau(C^{18}O) \Delta V(C^{18}O) T_{ex}}{1 - \exp(-5.27/T_{ex})}$$

where  $\tau(C^{18}O)$  is the optical depth of the  $C^{18}O$  line,  $\Delta V(C^{18}O)$  is the linewidth of  $C^{18}O$  line in  $\text{km s}^{-1}$ , and  $T_{ex}$  is the excitation temperature in K (see Table 5) estimated from our previous  $^{12}CO$  observations (Paper I). Since the clumps are far from S125 ( $\sim 20 \text{ pc}$ ) and it doesn't seem

TABLE 4. Observed parameters of the clumps.

Clump <sup>a</sup>	Position <sup>b</sup>				$C^{18}O(J=1-0)$			Comments <sup>c</sup>
	$\alpha(1950)$ (h m s)	$\delta(1950)$ (° ' )	l (°)	b (°)	$TR^*$ (K)	$\Delta V$ ( $\text{km s}^{-1}$ )	$V_{lsr}$ ( $\text{km s}^{-1}$ )	
B5	21 44 57	47 04.3	93.43	-4.67	0.42	1.7	5.1	L1031
C2	21 43 08	47 22.2	93.50	-4.33	0.58	1.9	3.8	L1035
C3	21 44 22	47 19.6	93.63	-4.50	0.88	1.6	3.2	L1045
	21 45 11	47 18.9	93.73	-4.60	0.75	1.1	3.7	L1045
	21 45 28	47 18.6	93.77	-4.63	1.29	1.2	3.7	L1045
	21 45 14	47 24.5	93.80	-4.53	0.56	1.5	3.8	L1045

note:

- a The names of clumps B5, C2, and C3 are quoted from Table 1 in Dobashi *et al.* (1992).  
 b Peak positions of the integrated intensity map of  $C^{18}O(J=1-0)$ .  
 c The asterisks (\*) in this column represent the most intense peak in each clump.  
 d Associated Lynds clouds (Lynds 1962).

TABLE 5. Derived properties of the clumps.

Clump	$T_{ex}$ <sup>a</sup> (K)	$\tau(C^{18}O)$	$N(C^{18}O)$ ( $10^{14} \text{cm}^{-2}$ )	$N(H_2)$ <sup>b</sup> ( $10^{21} \text{cm}^{-2}$ )	Mass <sup>c</sup> ( $M_{\odot}$ )	Size <sup>c</sup> (pc)
B5	9.1	0.075	6.4	5.2	...	$3.0 \times 1.5$
C2	12.1	0.068	10.8	7.0	610	$2.7 \times 2.7$
C3	9.2	0.24	15.0	8.6	960	$5.1 \times 1.3$

note:

- a The excitation temperature is estimated from our previous  $^{12}CO$  observations (paper I).  
 b The relationship between  $N(C^{18}O)$  and  $N(H_2)$  is assumed to be the same as that in Taurus region (Frerking, Langer, & Wilson 1982, see text). The ratio of  $\mu/m$  is taken to be 1.4, where  $\mu$  is the mean molecular weight and  $m$  is the  $H_2$  molecular mass.  
 c The mass and size are calculated by assuming a distance of 1 kpc (Walker 1959).

likely that they are strongly influenced by far-ultraviolet radiation like clouds in the Ophiuchus region (Nozawa *et al.* 1991), a relationship between  $N(C^{18}O)$  and  $N(H_2)$  is assumed to be the same as in Taurus (Frerking *et al.* 1982). From the derived value of  $N(H_2)$  and the area of the clumps, defined at one half of the peak intensity, the masses of clumps C2 and C3, in which five outflows are located, are estimated to be 610 and 960  $M_{\odot}$ , respectively. These values amount to  $\sim 70\%$  of the total mass derived from our previous  $^{13}CO$  observations ( $\sim 2200 M_{\odot}$ ). The mean numerical molecular densities,  $n(H_2)$ , are estimated to be  $\sim 1 \times 10^3 \text{ cm}^{-3}$  for both of C2 and C3 by dividing  $N(H_2)$  by the diameters of the clumps. The value is much smaller than those measured in nearby star forming regions observed with the 4 m telescope:  $n(H_2) > 1 \times 10^4 \text{ cm}^{-3}$  in Taurus and  $\rho$ -Oph regions for clumps with sizes from 0.2 to 0.5 pc in diameter (Mizuno *et al.* 1992). The difference may be caused by the effect of beam dilution, as the beam size of the 4 m telescope is  $\sim 0.8 \text{ pc}$  at a distance of 1 kpc.

Figure 9 shows an image of the five outflows superposed

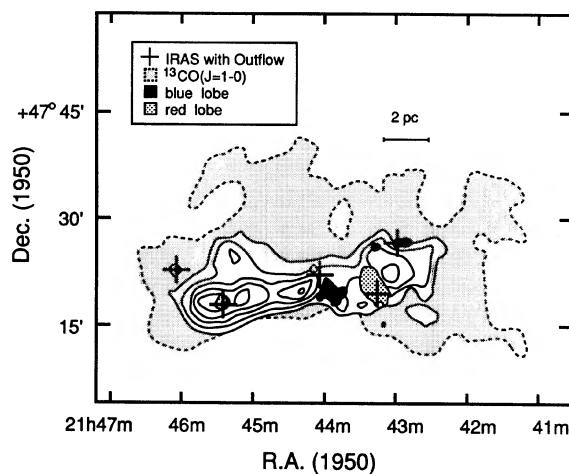


FIG. 9. Location of the five molecular outflows compared to the  $C^{18}O(J=1-0)$  integrated intensity map. Contours of the  $C^{18}O$  map (solid lines) are the same as Fig. 6.  $^{13}CO$  distributions are also shown by a contour of  $2.0 \text{ K km s}^{-1}$  (broken line). The four outflows studied in this paper are indicated by the lowest contours in Figs. 2, 4, 5, and 6, and their blue and red lobes are distinguished by different hatching. The red lobe of Elias 1-12 (21454+4718) are drawn by a contour of  $5 \text{ K km s}^{-1}$  (quoted from Levreault 1993). The associated *IRAS* sources are shown by the pluses.

on the  $C^{18}O$  map.  $^{13}CO$  distributions are also denoted in the figure by a contour of  $2.0 \text{ K km s}^{-1}$ . The outflow sources and the cold *IRAS* sources are located close to or within the  $C^{18}O$  cloud, although the outflows seem to avoid the strongest  $C^{18}O$  peaks. For instance, one notices a “hole” centered at R.A.(1950)  $\sim 21^{\text{h}}43.5^{\text{m}}$  and Dec.(1950)  $\sim +47^{\circ}20'$  where  $C^{18}O$  emission appears weaker, and the red lobe of Obj.9 partially overlaps the hole. This suggests an interaction between the outflow and the ambient gas, like in other star forming regions such as L1630 (Iwata *et al.* 1988),  $\rho$ -Oph (Mizuno *et al.* 1990), and L1221 (Umemoto *et al.* 1991).

### 3.3 Comparison of Young Stellar Objects with those in Taurus

The existence of the six protostar candidates and the five outflows strongly indicates that active star formation is occurring inside of the cloud, as was suggested in Paper I. The selected *IRAS* sources are located in denser parts ( $n[\text{H}_2] \sim 1 \times 10^3 \text{ cm}^{-3}$ ) of the cloud traced by  $C^{18}O$  emission rather than in the surrounding rarefied gas ( $n[\text{H}_2] \sim 4 \times 10^2 \text{ cm}^{-3}$ ) detected in  $^{13}CO$  (Fig. 9).

As we mentioned in Paper I, the relatively high luminosities of the *IRAS* sources (from  $4L_{\odot}$  up to  $160L_{\odot}$ ) suggest that the typical stellar mass is a little higher than that in the main Taurus cloud complex observed in  $^{13}CO$  (Fukui & Mizuno 1991), in which the maximum luminosity is  $\sim 10L_{\odot}$ . The typical  $C^{18}O(J=1-0)$  linewidth in clumps C2 and C3 is  $\sim 1.5 \text{ km s}^{-1}$ . This value is larger than that in Heiles Cloud 2 of the Taurus complex ( $\sim 0.5 \text{ km s}^{-1}$ ) observed with the same angular resolution of  $\sim 2.7$  arcmin. It is also larger than the value,  $\sim 1.0 \text{ km s}^{-1}$ , smoothed to a similar spatial resolution of  $\sim 0.8$  pc (the data were taken from Mizuno *et al.* 1992). This broad linewidth may induce relatively massive star formation in C2 and C3 since the mass accretion rate is proportional to the third power of the gaseous velocity dispersion (e.g., Shu *et al.* 1987). Alternatively, the linewidth we observed with the 4 m telescope could result from the contribution of smaller clumps with smaller linewidths. This possibility may be tested by future observations of  $C^{18}O$  in higher angular resolution.

Finally, we note that the search for young stellar objects in the cloud is not complete, because of high detection limits; in the FIR luminosity ( $\sim 10L_{\odot}$  in the *IRAS* survey), and in the K band ( $\sim 7$  mag, Elias 1978). The presence of the N-blue lobe near Obj.9 may indicate that some young stellar objects have not been discovered yet. Much deeper IR observations should be made to determine the physical properties such as luminosity functions and star-forming efficiencies of this cloud.

## 4. CONCLUSIONS

We made a survey for CO outflows in  $^{12}CO(J=1-0)$  and observations of the associated dense gas in  $C^{18}O(J=1-0)$  of the dark cloud complex near IC5146. Main conclusions are summarized as follows.

(1) Out of the six selected *IRAS* sources, four objects are newly identified to be outflow sources. We derived physical properties such as  $\text{H}_2$  column densities and masses of the outflows.

(2) We made  $C^{18}O(J=1-0)$  observations for a better estimate of mass of the cloud. Total mass of the cloud is  $\sim 1600M_{\odot}$  which is  $\sim 70\%$  of our previous estimated ( $\sim 2200M_{\odot}$ ) measured with  $^{13}CO(J=1-0)$  emission. The cloud mass is similar to that of Taurus cloud complex.

(3) Five outflow sources are located where  $C^{18}O$  emission is higher than  $0.2 \text{ K km s}^{-1}$ , and the sources have much higher FIR bolometric luminosities (from  $< 5L_{\odot}$  up to  $160L_{\odot}$ ) than those in Taurus cloud complex ( $< 10L_{\odot}$ ).

We are very grateful to Drs. Hideo Ogawa and Akira Mizuno for their great efforts in maintaining the new 4 m telescope during the observations. Thanks are due to Drs. Koji Sugitani and Jean-Philippe Bernard for their helpful comments. This work was financially supported by the Grant-in-Aid for specially promoted research No. 01065002 and the Grant-in-Aid for international scientific research No. 02044064 in the Ministry of Education, Science, and Culture.

### APPENDIX: $^{12}CO$ AND $\text{H}_2$ COLUMN DENSITIES IN THE WING COMPONENT OF THE OUTFLOWS

In order to derive the column densities of  $^{12}CO$ , we assumed that radiation field satisfies local thermal equilibrium. The column densities of  $^{12}CO$  are calculated according to

$$N(^{12}CO) = 4.34 \times 10^{13} T_{\text{ex}} \exp(5.53/T_{\text{ex}}) \int \beta^{-1} T_R^* dv, \quad (\text{A1})$$

where  $T_{\text{ex}}$  is the excitation temperature in K estimated from the antenna temperature, and  $\int \beta^{-1} T_R^* dv$  is the wing intensity integrated over the wing component in  $\text{K km s}^{-1}$ .  $\beta$  is defined from the  $^{12}CO$  optical depth,  $\tau(^{12}CO)$ , as a function of LSR velocity:

$$\beta = \frac{1 - \exp[-\tau_v(^{12}CO)]}{\tau_v(^{12}CO)}. \quad (\text{A2})$$

In this paper, we assumed uniform  $\tau(^{12}CO)$  of  $\sim 4$  at all velocities and in each outflow lobes. This value is based on the following ratio:

$$\frac{\int T_R^*(^{12}CO) dv}{\int T_R^*(^{13}CO) dv} = \frac{\int 1 - \exp[-\tau_v(^{12}CO)] dv}{\int 1 - \exp[-\tau_v(^{13}CO)] dv} \approx 20, \quad (\text{A3})$$

which was measured in the red lobe of Elias 1-12 (Levreault 1983). We take  $\tau(^{12}CO) = 89 \times \tau(^{13}CO)$  under the assumption that the  $^{12}CO$  to  $^{13}CO$  abundance ratio is equal to the terrestrial value. The column densities of  $\text{H}_2$  molecules are estimated using  $[\text{H}_2]/[^{12}CO]$  ratio of  $\sim 1 \times 10^4$  (Frerking *et al.* 1982).

## REFERENCES

- Beichman, C. A., Myers, P. C., Emerson, J. P., Harris, S., Mathieu, R., Benson, P. J., & Jennings, R. E. 1986, *ApJ*, 307, 337
- Dobashi, K., Yonekura, Y., Mizuno, A., & Fukui, Y. 1992, *AJ*, 104, 1525 (Paper I)
- Elias, J. H. 1978, *ApJ*, 223, 859
- Erickson, N. R., Goldsmith, P. F., Novak, G., Grosslein, R. M., Viscuso, P. J., Erickson, R. B., & Predmore, C. R. 1992, *IEEE Transactions on Microwave Theory and Techniques*, 40, No. 1, 1
- Frerking, M. A., Langer, W. D., & Wilson, R. W. 1982, *ApJ*, 262, 590  
IRAS Point Source Catalog, 1988, Joint IRAS Science Working Group (U.S. GPO, Washington, DC)
- Fukui, Y. 1989, in *Proceedings of the ESO Workshop on Low Mass Starformation and Pre-Main Sequence Objects*, edited by B. Reipurth (ESO, Garching), p. 95
- Fukui, Y., & Mizuno, A. 1991, in *Fragmentation of Molecular Clouds and Star Formation*, IAU Symposium No. 147, edited by E. Falgarone *et al.* (Reidel, Dordrecht), p. 275
- Fukui, Y., Iwata, T., Mizuno, A., Bally, & Lane, A. 1992, in *Protostars and Planets III*, edited by E. Levy (Arizona University, Tucson) (in press)
- Israel, F. P. 1977, *A&A*, 60, 223
- Iwata, T., Fukui, Y., & Ogawa, H. 1988, *ApJ*, 325, 372
- Lada, C. J. 1985, *ARA&A*, 23, 267
- Lada, C. J., & Elmegreen, B. G. 1979, *AJ*, 84, 336
- Levreault, R. M. 1983, *ApJ*, 265, 855
- Levreault, R. M. 1988, *ApJ*, 330, 897
- Lynds, B. T. 1962, *ApJS*, 7, 1
- McCutcheon, W. H., Roger, R. S. & Dickman, R. L. 1982, *ApJ*, 256, 139
- Milman, A. S., Knapp, G. R., Knapp, S. L., & Wilson, W. J. 1975, *AJ*, 80, 101
- Mizuno, A., Fukui, Y., Iwata, T., & Nozawa, S. 1990, *ApJ*, 356, 184
- Mizuno *et al.* 1992 (in preparation)
- Myers, P. C., Fuller, G. A., Mathieu, R. D., Beichman, C. A., Schild, R. E., & Emerson, J. P. 1987, *ApJ*, 319, 340
- Nozawa, S., Mizuno, A., Teshima, Y., Ogawa, H., & Fukui, Y. 1991, *ApJS*, 77, 647
- Ogawa, H., Mizuno, A., Hoko, H., Ishikawa, H., & Fukui, Y. 1990, *Internat. J. Infrared Milimeter Waves*, 11, 717
- Riegel, K. W. 1967, *ApJ*, 148, 87
- Roger, R. S., & Irwin, J. A. 1982, *ApJ*, 256, 127
- Shu, F. H., Adams, F. C., & Lizano, S. 1987, *ARA&A*, 25, 23
- Snell, R. L. 1987, in *Star Forming Regions*, edited by M. Peimbert and J. Jugaku (Reidel, Dordrecht), p. 213
- Umemoto, T., Hirano, N., Kameya, O., Fukui, Y., Kuno, N., & Takakubo, K. 1991, *ApJ*, 377, 510
- Walker, M. F. 1959, *ApJ*, 130, 57
- Wilking, B. A., Harvey, P. A., & Joy, M. 1984, *AJ*, 89, 496
- Wilking, B. A., & Lada, C. J. 1983, *ApJ*, 274, 698